Research Square

Preprints are preliminary reports that have not undergone peer review.
They should not be considered conclusive, used to inform clinical practice,
or referenced by the media as validated information.

Annona muricata Leaves Extract as Sustainable Corrosion Inhibitor to Improve Corrosion Resistance on API 5L Steel in Sulfuric Acid Media: Experimental, Thermodynamic and DFT Analysis

Siska Prifiharni
University of Indonesia
Rini Riastuti
rini.riastuti@yahoo.com
University of Indonesia
Gadang Priyotomo
National Research and Innovation Agency
Johny Wahyuadi Mudaryoto
University of Indonesia

Research Article

Keywords: green inhibitor, A. muricata, DFT analysis, XPS, Thermodynamic

Posted Date: November 26th, 2026

DOI: https://doi.org/10.21203/rs.3.rs-11752790/v1

License: This work is licensed under a Creative Commons Attribution 4.0 International License.
Read Full License

Additional Declarations: No competing interests reported.

Annona muricata Leaves Extract as Sustainable Corrosion Inhibitor to Improve Corrosion Resistance on API 5L Steel in Sulfuric Acid Media: Experimental, Thermodynamic and DFT Analysis

Siska Prifiharni[1,2*], Rini Riastuti[1*], Gadang Priyotomo[2], Johny Wahyuadi Mudaryoto[1]

[1]Metallurgy and Material Engineering Department, Faculty of Engineering, University of Indonesia, Depok, Indonesia
[2]Research Center for Metallurgy, National Research and Innovation Agency, Tangerang Selatan, Indonesia

*Corresponding author : siska.prifiharni41@ui.ac.id; rini.riastuti@yahoo.com

ABSTRACT

Corrosion is one of the biggest challenges in the oil and gas industry, particularly for API 5L steel pipes exposed to acidic environment. Therefore, an effective corrosion inhibitor especially in environmental friendly is mandatory to prevent the steel from corrosion. This study is focused on exploring *A. muricata* leaves extract (AMLE) to prevent corrosion on mild steel in H_2SO_4 environment. The electrochemical studies show the highest inhibition efficiency was 91% at 1000 ppm and act as mixed-type corrosion inhibitors. The formation of protective layers on the surface was shown by secondary electron microscope (SEM) significantly reducing the damage. From XPS results there is no sign of damaging corrosion products were detected. The adsorption of AMLE followed Langmuir isotherm indicating the mixed-type adsorption mechanism.

Keyword : green inhibitor, *A. muricata*, DFT analysis, XPS, Thermodynamic

1. Introduction

Corrosion is a phenomenon of material degradation that occurs spontaneously as a result of chemical or electrochemical interactions between metals and their environment [1] . On a global scale, corrosion is not just a technical issue, but a significant threat to national economies and public safety. According to a report by NACE International [2] , global economic losses due to corrosion are estimated at $2.5 trillion USD annually, equivalent to 3% to 4% of the Gross Domestic Product (GDP) of industrialized nations. The oil and natural gas sectors are the primary contributors to these statistics, due to its heavy reliance on metal infrastructure exposed to extreme environments.

Low-carbon steel, particularly the API 5L grade, is the most widely used standard material in the pipeline industry for transporting crude oil, natural gas, and petrochemical products. The selection of API 5L steel is based on a combination of superior mechanical properties, such as high tensile strength, toughness, and good weldability [3,4] . However, the main limitation of this steel is its susceptibility to corrosion when exposed to corrosive electrolytes [5]. Structural failure in API 5L pipelines due to corrosion can lead to severe environmental damage through toxic substance leaks, explosions, and operational shutdowns that require costly maintenance [6]. Therefore, protecting API 5L steel is a major concern in asset management in the energy industry.

During their operations, API 5L steel pipes are frequently exposed to strong acid solutions, one of which is sulfuric acid (H_2SO_4). Sulfuric acid is used widely in acid pickling, a process that cleans metal surfaces of oxide scale and rust prior to coating, galvanizing, or painting [7,8]. Although sulfuric acid is effective as a cleaning agent, its highly aggressive nature causes metals to dissolve very rapidly. Hydrogen ions (H^+) in the acid solution act as oxidizing agents that accelerate the anodic reaction (the dissolution of iron into Fe^{2+} ions) and the cathodic reaction (the reduction of hydrogen ions into H_2S gas) [9]. Without additional protection, the steel surface will suffer drastic thinning and localized corrosion (pitting) that is difficult to detect visually but fatal to the structural integrity [10].

One of the most effective and economical strategies for controlling the rate of corrosion in acidic environments is the addition of corrosion inhibitors [11,12]. Inhibitors are chemical compounds added in small concentrations to corrosive media to inhibit the interaction between the metal and the environment. Traditionally, the corrosion inhibitors used are synthetic organic compounds containing elements such as nitrogen (N), oxygen (O), phosphorus (P), and sulphur (S), which have lone pairs of electrons [13,14] .

However, the use of conventional synthetic inhibitors has come up against significant criticism over the past decade. Many of these compounds are highly toxic, non-biodegradable, and can accumulate in the food chain, ultimately posing a threat to aquatic ecosystems and human health [15,16] . This has caused a shift in the research focus on Green Corrosion Inhibitors. These inhibitors are derived from plant extracts, agricultural waste, and natural polymers, offering a high safety profile, low production costs, and wide availability in nature. Several studies have been conducted using plant extracts derived from tree trunks [17] , roots [18] , fruit peels [19] , leaves [20], flowers [21] , and seeds [22,23] . These materials are rich in antioxidants, ascorbic acid,

tocopherols, carotenoids, phenolic compounds, alkaloids, flavonoids, tannins, cellulose, and polycyclic compounds. These studies have demonstrated the effectiveness of these extracts in reducing the corrosion rate of materials, particularly low-carbon steel. Some studies also show that plant extracts can achieve high inhibition efficiency through the adsorption of heteroatom-rich molecules (O, N, S) and the formation of a protective film that can inhibit electron charge transfer, thereby enhancing protection against corrosion[24–26] .

There are several research on plant extract as corrosion inhibitor, such as *Pulsatilla chinensis* extract [27] on Q235 carbon steel in 0.5 M H_2SO_4 achieved an efficiency of 95.3% (298 K), confirmed as a mixed-type inhibitor using the Langmuir adsorption approach and physicochemical characterization (physisorption + chemisorption), as evidenced by electrochemical methods, surface characterization (SEM/AFM/XPS/ATR-FTIR). In another study, *Cymbopogon citratus* [28] (lemongrass), the inhibition efficiency increased to ~92% at 25 °C (0.1 M H_2SO_4), as determined by EIS, Tafel polarization, and mass loss tests. The analysis results showed a general trend of decreasing efficiency as temperature increased, indicating poor stability of the adsorption film at higher temperatures. In the recent studies, Gusti, et.al [29] investigated about *Macaranga gigantea sap* extract achieved over 80% corrosion inhibition at 333 K on mild steel in 0.75M H_2SO_4.

A literature review said that more than two hundred bioactive compounds have been reported to be present in A. muricata. The predominant compounds are acetogenins, followed by alkaloids, phenols, and other compounds. The leaves and seeds are the primary plant parts studied, likely because they are the parts most commonly used in traditional medicine [30]. A. muricata leaves have the highest concentration of alkaloids [31,32], although these compounds are also found in the roots, stems, and fruits. The alkaloids reported in A. muricata are primarily of the isoquinoline, aporphine, and protoberberine types [33]. Important phenolic compounds found in the leaves of A. muricata include quercetin [34] and gallic acid [35]. The presence of flavonoids and lipophilic antioxidant compounds such as tocopherols and tocotrienols has been reported in the fruit pulp. Phenolic compounds are considered the primary phytochemicals responsible for antioxidant activity. Therefore, A. muricata leaves extract can be used to improved corrosion properties of mild steel.

This study was to investigated the effect of A. muricata leaves extract on API 5L steel especially in H_2SO_4 environment using electrochemical measurement such as potentiodynamic

polarization and electrochemical impedance spectroscopy. The surface of metals after exposed to the corrosive environment also characterized using several characterization such as secondary electron microscope (SEM), atomic force microscope (AFM), and x-ray photoelectron spectroscopy (XPS). This comprehensive method describes a thorough process for the adsorption of these chemicals onto the steel surface in addition to deepening knowledge of the inhibition activity.

2. Materials and Method

2.1 Materials

The material used in this study was API 5L steel. The chemical composition of the steel were: 0.21% C, 0.79% Mn, 0.03% P, 0.006% Si, and balance Fe. The steel was then cut into 10 x 10 mm pieces with a thickness of 3 mm, connected with wire, mounted, and polished using abrasive paper with grits ranging from #120 to #1200 for the polarization testing process.

2.2 Preparation of Extraction

Annona Muricata leaves were collected from Tangerang Selatan, Indonesia. The leaves were rinsed, dried, and chopped into a fine powder. After that, 25 gr of fine powder was immersed in 250 ml ethanol (1:10) for 24 hr. The soursop leaf mixture is then filtered. The filtrate is then concentrated using a rotary evaporator. The concentrate obtained from the rotary evaporator is ready for use as an inhibitor (**Figure 1**).

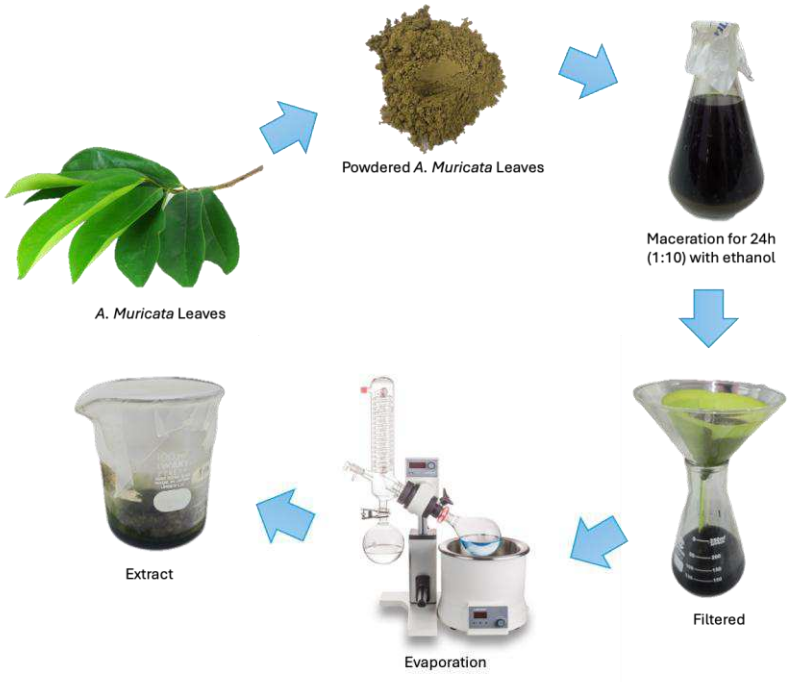

Figure 1. Schematic process of *A. Muricata* leaves extraction

2.3 Electrochemical Measurement

The electrochemical testing in this study included Electrochemical Impedance Spectroscopy (EIS), which was performed to quantitatively analyse the performance of the protective layer and the inhibition mechanism of the inhibitor, as well as Tafel polarization measurements to determine the corrosion rate and corrosion potential (E_{corr}) before and after the addition of the inhibitor. Prior to the EIS and Tafel tests, the open-circuit potential (OCP) was measured to ensure that the interaction between the metal and the electrolyte solution had stabilized before more detailed corrosion rate measurements were taken. The electrochemical tests were conducted in a three-electrode system consisting of a carbon steel electrode, a graphite electrode, and a saturated calomel electrode (SCE). Prior to testing, the working electrode was immersed in the test solution for 15 minutes to stabilize the OCP. For EIS, the frequency range was set from 10^5 to 10^{-2} Hz with an AC excitation amplitude of 10 mV. Then, a Dynamic Polarization Potential test was performed at a scan rate of 1 mV/s, scanning from −0.25 V to 0.25 V relative to the OCP.

2.4 Surface Morphology

The polished steel samples were immersed for 72 hours in 1M H_2SO_4 solutions containing 1000 ppm *A. muricata* extract and without the addition of inhibitor. After the removal, the samples were immediately rinsed with distilled water, gently swab with tissue towel, and dried using hair dryer. Next, the steel samples coated with the inhibitor were collected and characterized using SEM-EDS (Jeol JSM-IT200) to examine the surface morphology of the steel samples before and after the addition of the inhibitor. The collected samples also characterized using AFM to resolves the 3D structure of metal surface using Park Systems NX10. The XPS analysis was conducted using JEOL JPS 9030 to analysed the oxide film on the metal surface.

2.5 Characterization of Extract

The soursop leaf extract was then characterized using FTIR (Bruker) to identify the functional groups present in the extract with range wavenumber from 500 to 4000. UV-Vis using Hitachi UH5300 characterization was also performed to identify the molecular compounds present in the soursop leaf extract. In addition, GC-MS characterization was conducted to identify and quantify the types and amounts of organic compounds.

3. Results and Discussion

3.1 Extract Characterization

Soursop leaf extract was characterized using UV-Vis and FTIR spectroscopy. **Figure 2**a shows the UV-Vis spectrum, which shows the absorbance (Abs) versus wavelength in the range from 200 nm to 900 nm. The figure shows very intense and sharp absorption in the wavelength range of 200 – 240 nm. The highest peaks are detected around 207 – 210 nm and 224 nm. Peaks at 200–240 nm indicate the presence of a characteristic $\pi \rightarrow \pi^*$ electronic transition from an isolated double bond system C = C or a heterocyclic structure [36,37] . In soursop leaves, this band confirms the presence of alkaloid compounds (such as annonaine or isoquinoline alkaloids) as well as acetogenin skeletons (annonaceous acetogenins) containing unsaturated lactone rings. The 260 - 290 nm range refers to absorption band II (Band II) produced by aromatic ring A (the benzoyl system) in the flavonoid structure. The slope in the 300 – 350 nm range corresponds to absorption band I (Band I), which originates from the B ring (cinnamoyl system) in flavonoids such as quercetin or rutin derivatives, which are abundant in soursop leaves [38].

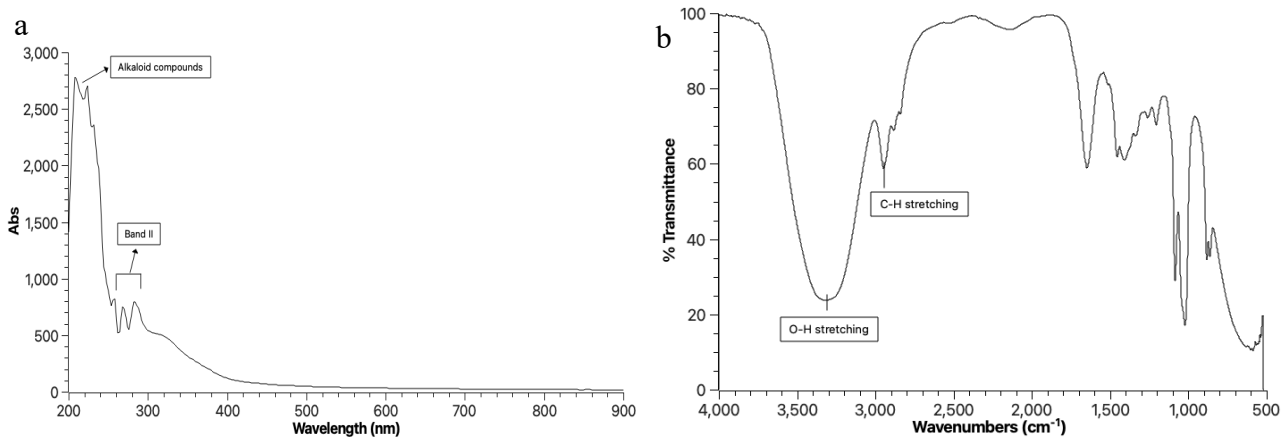

Figure 2. UV-Vis and FTIR analysis of *A. Muricata* Leaves Extract

Functional group analysis using Fourier-transform infrared (FTIR) spectroscopy was conducted to identify active phytochemical molecules in soursop leaf extract that have potential as corrosion inhibitors. **Figure 2**b shows the FTIR spectrum, which plots transmittance (%) against wavenumber from 4,000 cm^{-1} to 500 cm^{-1}. The FTIR spectrum of the extract shows several characteristic absorption bands that reflect the presence of phenolic compounds, flavonoids, tannins, and alkaloids. A wide and intense absorption band was detected at a wavenumber around 3.325 cm^{-1}, indicating the presence of hydroxyl bond stretching (O-H stretching) and amino groups. Furthermore, the peak that appears at around 2945 cm^{-1} indicates the stretching of aliphatic C-H bonds from the methyl ($-CH_3$) and methylene ($-CH_2$) groups, which represent the long-chain hydrocarbon backbone in secondary metabolites such as acetogenins [39,40] . The absorption at a wavenumber of 1.645 cm^{-1} indicates the presence of a C=O (carbonyl) stretch or a conjugated aromatic C=C stretch from the benzene rings that construct the basic structure of the flavonoid [41,42] . These functional groups of -OH, C-H, -CH (-CH3 or -CH2), C=C, C-O, and C-C may be due to the Loliolide, hexadecanioc acid, m-Guaiacol, and 4-((1E)-3-Hydroxy-1-propenyl)-2-methoxyphenol that were detected by GC-MS in *A. Muricata L*. extract (**Figure 3**).

3.2 Electrochemical Characterization

3.2.1 Tafel Polarization

The corrosion inhibitor performance of *A. muricata* leaf extract on steel in a sulfuric acid environment was examined using the PDP technique at various concentrations and temperatures. This approach quantifies the current density associated with the working electrode in relation to the reference electrode. The analysis of the polarization curves permits an evaluation of the electrochemical attributes of the metal in the corrosive setting. **Figure 4** shows Tafel polarization diagram of soursop leaves extract at various concentration. The polarization parameters such as E_{corr} (corrosion potential), corrosion current density (i_{corr}), anodic Tafel slope ($ß_a$), cathodic Tafel

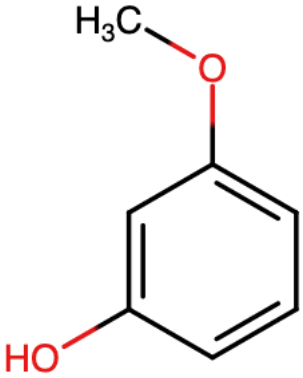

m-guaiacol

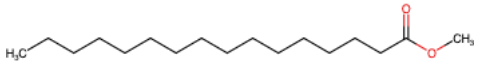

n-hexadecanioc acid

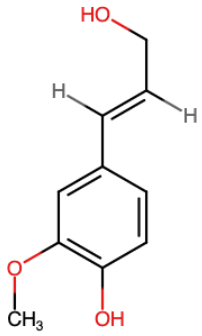

4-((1E)-3-Hydroxy-1-propenyl)-2-methoxyphenol

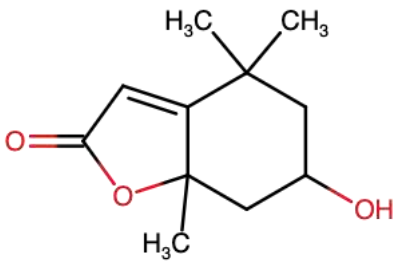

Loliolide

Figure 3. Phytochemical structure found in *A. Muricata* leaves extract

slope ($ß_c$), corrosion rate (CR), and inhibition efficiency (η) were shown in **Table 1**. The inhibition efficiency were calculated using following equation

$$\eta = \left(1 - \frac{i_{corr}}{i^0_{corr}}\right) x\ 100\% \quad (1)$$

Where η represents inhibition efficiency, i_{corr} represents corrosion current density with inhibitor, and i^0_{corr} represents corrosion current density without inhibitor.

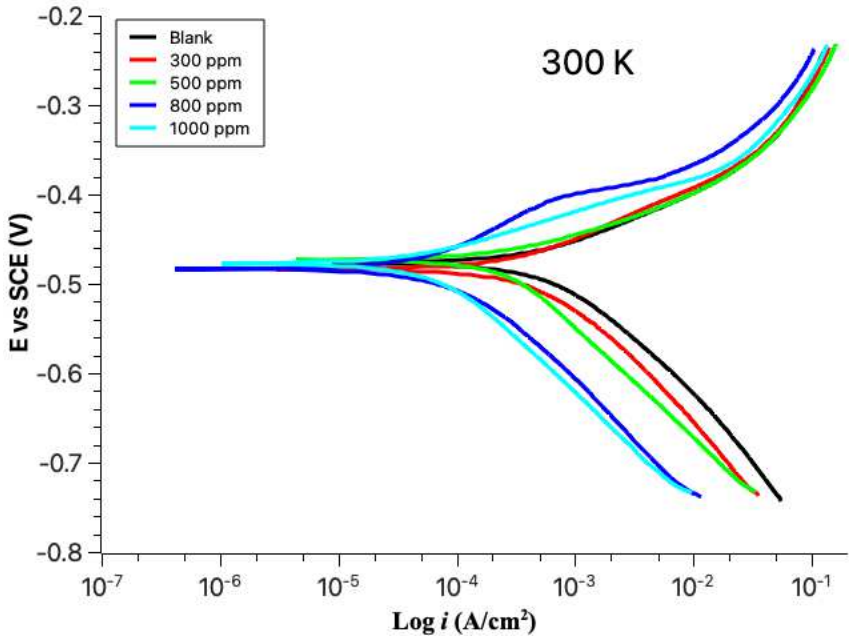

Figure 4. Tafel polarization of API 5L without and with addition of *A. Muricata* extract in H_2SO_4 environment.

From the polarization curve shown in **Figure 4**, a slight shifted in the direction of i_{corr} to the left can be observed, indicating a decrease in the corrosion rate after the addition of *A. muricata* extract. The polarization results presented in **Table 1** show a remarkable decrease in corrosion current density subsequent to the addition of *A. muricata* extract. The decrease in current density is directly linked to the decrease in corrosion rate. According to data from the polarization results, the lowest corrosion rate was 0.41 mmpy at a concentration of 1000 ppm of *A. Muriata* extract. This reduction in corrosion rate also correlated with the inhibition efficiency (η) of the *A. muricata* extract, reaching 91%. This indicates that the presence of this inhibitor can reduce both cathodic and anodic current densities, thereby preventing anodic dissolution in steel and hydrogen evolution reactions in an acidic environment [43–45] . The difference in corrosion potential caused by the addition of *A. muricata* extract was only about 10 mV. This indicates that the *A. muricata* extract act as a mixed-type inhibitor for API 5L steel in sulfuric acid environment, since the E_{corr} difference was less than 85 mV [46–48] .

Table 1. Polarization parameters of *A. Muricata* extract on API 5L steel in H_2SO_4 environment.

C_{inh} (ppm)	$ß_a$ (V/decade)	$ß_c$ (V/decade)	i_{corr} (mA)	E_{corr} (mV)	CR (mmpy)	η
Blank	0.065	0.120	0.591	-477	4.59	
300	0.066	0.111	0.380	-483	2.94	36%
500	0.046	0.127	0.266	-473	1.97	57%
800	0.095	0.113	0.085	-483	0.66	86%
1000	0.044	0.105	0.052	-477	0.41	91%

3.2.2 Electrochemical Impedance Spectroscopy

Electrochemical Impedance Spectroscopy (EIS) represents a non-destructive and exceptionally informative methodology for the investigation of corrosion mechanisms and passivation phenomena associated with metals and their alloys. This study examines the corrosion behaviour of A. Muricata leaves extract on API 5L steel in H_2SO_4 environment. **Figure 5** shows the EIS diagram of API 5L steel without and with addition of *A. Muricata* leaves extract as corrosion inhibitor in H_2SO_4 environment. A Nyquist plot depicts a semicircle; as the diameter of the semicircle grows larger, it suggests the formation of passivation on the metal surface [44] . As seen in the **Figure 5**a, the semicircle of API 5L steel after addition of *A. Muricata* leaves extract was grow larger. With increasing the concentration of *A. Muricata* leaves extract in H_2SO_4 environment, the radius of semicircle impedance improve dramatically. A bode plot, as shown in **Figure 5Error! Reference source not found.**b also shows higher magnitude of impedance after addition of *A. Muricata* leaves extract compared to the blank one. The phase angle plot displays the phase shift between the applied voltage and current. The phase angle of blank sample shows narrow and low peak, meanwhile a inhibited steel shows boarder and higher peak of phase angle. A broadening of the phase angle peak across the mid-frequency range indicates the formation of a stable, highly capacitive protective layer that behaves like a constant phase element (CPE) [49,50] .

Figure 5c show an equivalent circuit diagram used in this study for analysing the EIS diagram. The impedance parameter obtained from equivalent circuit was shown in **Table 2**. R_s represents the solution resistance of H_2SO_4, R_{ct} represents the charge transfer resistance of the steel, and C_{dl} represents the capacitance double layer of steel/solution interface. C_{dl} is the CPE of the electrical double layer at the metal/electrolyte interface in the corresponding electrical circuit. The impedance of the CPE, which is a non-ideal capacitor in the EIS data, is expressed as follows

$$Z_{CPE} = \frac{1}{Y_0(j\omega)^n} \quad (2)$$

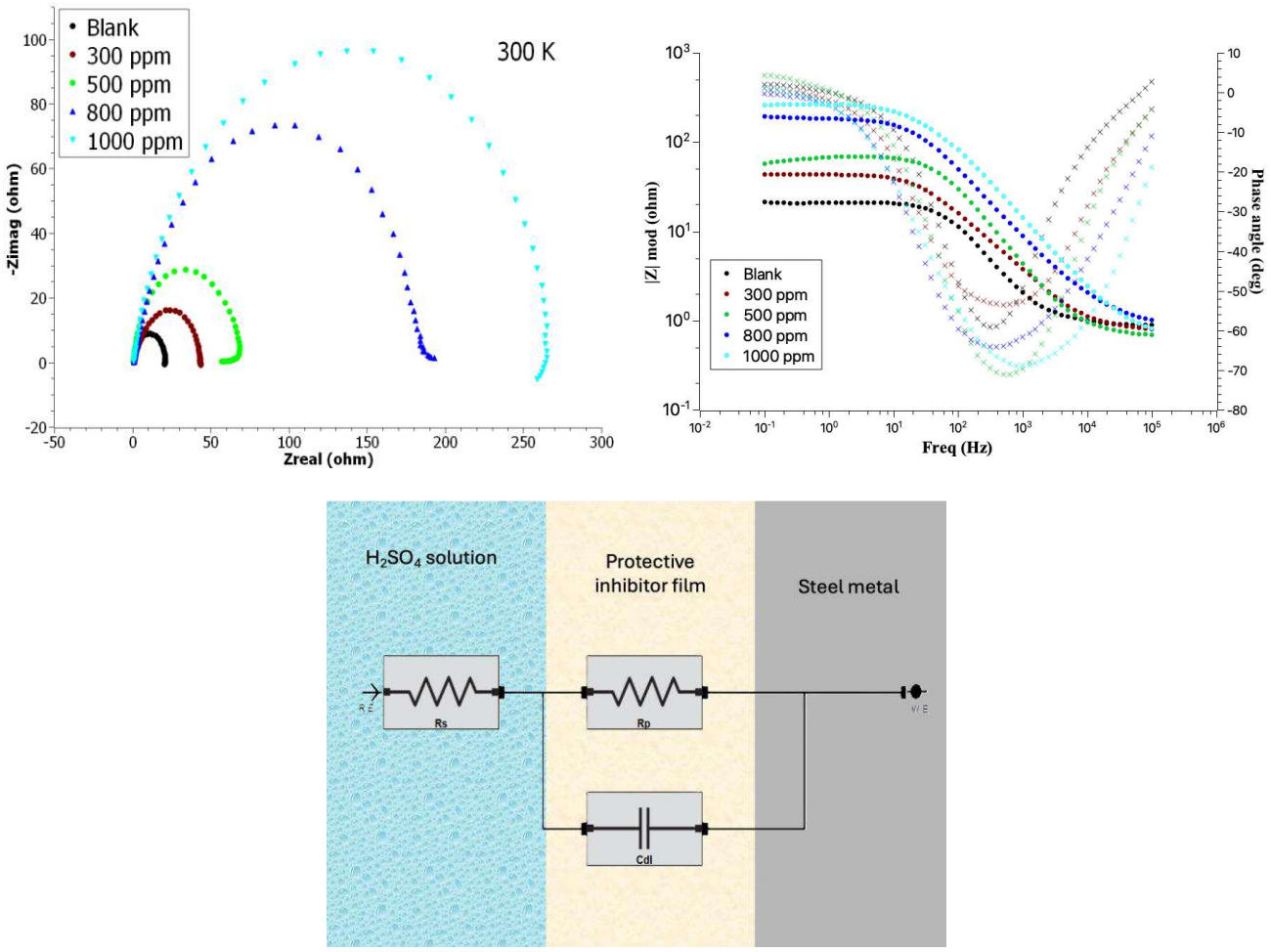

Figure 5. EIS of API 5L with and without addition of *A. Muricata* leaves extract in H_2SO_4 (a) Nyquist, (b) Bode, (c) equivalent circuit

Where Y0 is the CPE constant, n is the phase shift which provides information about homogeneity of surface on by surface roughness, porosity barrier formation, and inhibitor adsorption with rhe value ($-1 \leq n \leq 1$). The capacitance double layer is obtained from Eq.2 which represented in **Table 2**.

$$C_{dl} = (QR_{ct}^{1-n})^{1/n} \quad (1)$$

Table 2 reveals a higher R_{ct} values of the steel following the addition of *A. Muricata* leaves extract, proving to the creation of protective passive layer on metal/solution interface [51–53] . On the other hand, Cdl values decrease with an increase of *A. Muricata* extract likely due to a decrease in the local dielectric constant and/or an increase in the thickness of a protective layer at the electrode surface, which would therefore enhance the corrosion resistance of API 5L steel in 1 M

H_2SO_4 solution [54,55] . This suggest that it has a thicker electrical double layer due to the displacement of corrosive molecule with organic inhibitor molecule at the steel/solution interface. The improvement of R_{ct} values in higher concentration of A. Muricata extract implies that the adsorption of organic molecule of A. Muricata extract has taken places on the metal surface which prevents the corrosive electrolyte from coming into direct contact with the metal surface [56,57] . As seen in **Table 2** that At 1000 ppm of *A. Muricata* extract shows the highest R_{ct} values, with 265.4 Ω. As a results, the inhibition efficiency of A. Muricata extract reaching an optimal value to 92% at 1000 ppm.

Table 2. Electrochemical impedance data of API 5L in H_2SO_4 with and without addition of *A. Muricara* extract

C_{inh}	Rp (ohm)	Rs (ohm)	Y_0 ($\mu F.S^*s^a$)	n	Cdl ($\mu F/cm^2$)	η (%)
Blank	20.33	0.92	223.1	0.90	221.1	
300 ppm	43.08	0.83	218.8	0.82	210.3	53%
500 ppm	68.64	0.69	92.9	0.89	89.1	70%
800 ppm	185.24	1.07	71.6	0.85	72.5	89%
1000 ppm	265.42	0.67	56.6	0.81	51.8	92%

3.2.3 Effect of Temperature

The polarization studies on the corrosion rate of steel in a sulfuric acid environment with varying concentrations and temperature was investigated to understand the inhibition adsorption and estimate the activation energy, which is shown in

Figure *6*. As seen in

Figure *6*, a higher temperature resulting in shifting direction of i_{corr} to the right in each concentration of inhibitor,

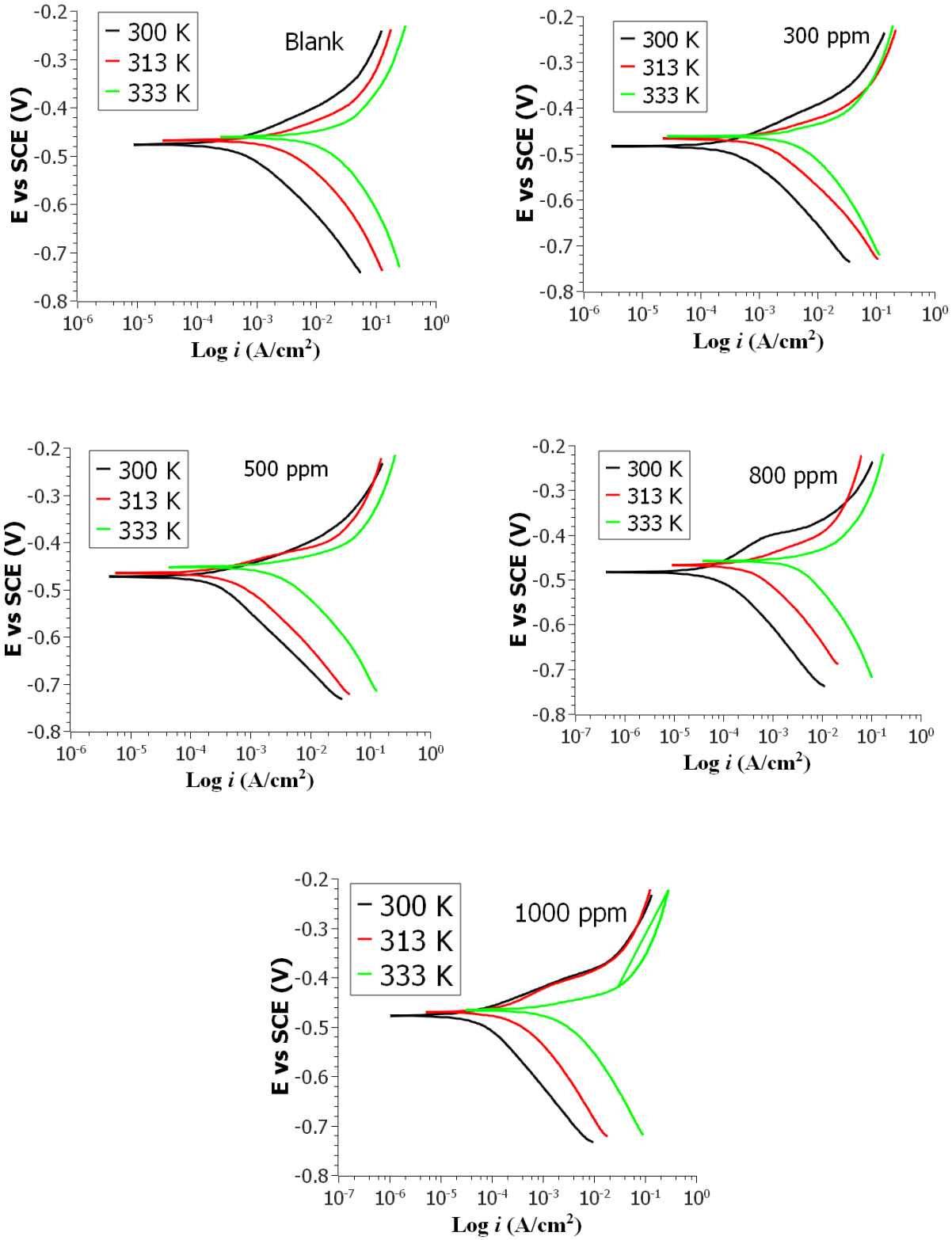

Figure 6. Polarization of API 5L at various temperature in H_2SO_4 environment with different *A. Muricata* leaves extract concentration.

which makes the i_{corr} increase at higher temperature. The increase of i_{corr} also correlated with the increase of corrosion rate.

The results of the electrochemical parameters of soursop leaf extract at temperatures ranging from 300 to 333 K are shown in **Table 3**. It is found that the corrosion rate of API 5L steel was increase when the temperature increase. This is because when the temperature rising, the heat gives particles more energy, causing them to move faster and collide more often which can speeds up electrochemical reactions and the movement of corrosive particles [58,59]. Adding *A. muricata* extract to an H_2SO_4 solution can reduce the corrosion rate of API 5L steel. However, as the temperature rises (300 – 333 K), the inhibition efficiency of the *A. muricata* extract also decreases from 91% to 89% at 1000 ppm. This decrease can be caused by desorption of inhibitor molecule on the metal surface due to higher thermal energy. As the inhibitor film thins or breaks down, the metal loses its protective barrier, lowering the inhibition efficiency [60].

Table 3. Electrochemical parameters of *A. Muricata* leaves extract as corrosion inhibitors at various temperature.

Temperature (K)	C_{inh} (ppm)	$ß_a$ (V/decade)	$ß_c$ (V/decade)	i_{corr} (mA)	E_{corr} (mV)	CR (mmpy)	η (%)
300	Blank	0.065	0.120	0.591	-477	4.59	
	300	0.066	0.111	0.380	-483	2.94	36%
	500	0.046	0.127	0.266	-473	1.97	57%
	800	0.095	0.113	0.085	-483	0.66	86%
	1000	0.044	0.105	0.052	-477	0.41	91%
313	Blank	0.064	0.114	2.490	-468	19.32	
	300	0.055	0.127	1.430	-467	11.11	42%
	500	0.062	0.129	0.553	-465	4.29	78%
	800	0.053	0.116	0.393	-467	3.05	84%
	1000	0.054	0.135	0.260	-465.4	2.02	90%
333	Blank	0.079	0.178	15.440	-461.3	119.80	
	300	0.094	0.208	7.591	-463	58.89	51%
	500	0.077	0.183	5.706	-455.3	44.27	63%
	800	0.069	0.171	4.583	-458.9	35.56	70%
	1000	0.038	0.120	1.770	-465.8	13.74	89%

Arrhenius plots were used to calculate the corrosion reactions theoretical activation energy, or E_a. A common way to express the Arrhenius equation is as

$$\ln(i_{corr}) = \ln(\mathrm{A}) + \left(-\frac{\mathrm{E_a}}{\mathrm{RT}}\right) \quad (2)$$

Where i_{corr} is corrosion current density of the steel, E_a is the activation energy of corrosion reaction, T is absolute temperature, R is the universal gas constant and A is the Arrhenius pre-exponential factor. Plotting ln(i_{corr}) with 1/T provides a straight line that can be used to calculated the activation energy of corrosion reaction without and with inhibitor. To calculate the enthalpy (ΔH_a) and enthropy (ΔS_a), alternative Arrhenius plots were used using eq. 4

$$\ln\left(\frac{i_{corr}}{T}\right) = \ln\left(\frac{R}{Nh}\right) + \left(\frac{\Delta S_a}{\mathrm{R}}\right) - \left(\frac{\Delta H_a}{RT}\right) \quad (3)$$

Where N is avogadro's number and h represents planck's constant. **Error! Reference source not found.** shows Arrhenius plot in the absence and the presence of *A. Muricata* extract in H_2SO_4 environment.

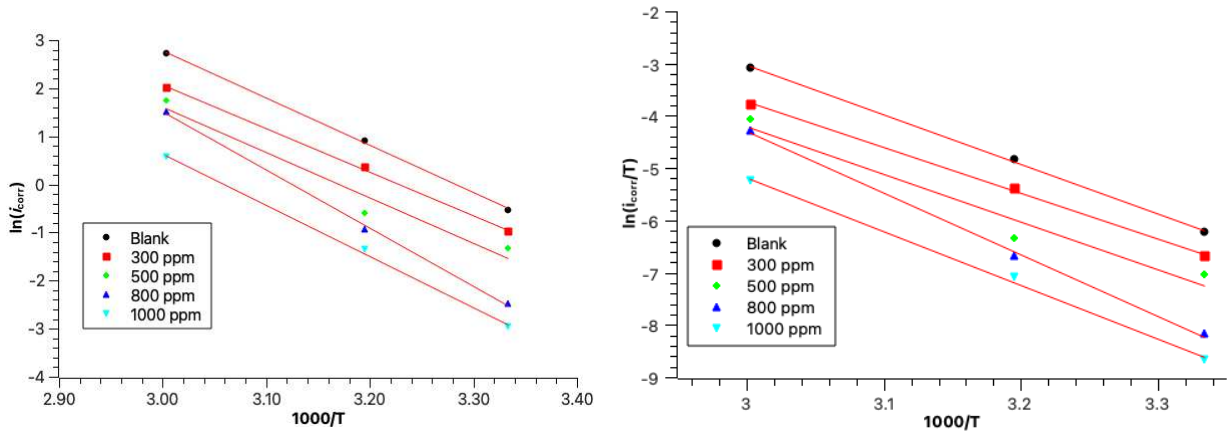

Figure 7. (a) Arrhenius plot (b) and Arrhenius plot of ln(icorr/T) vs 1000/T of *A. Muricata* extract on API 5L steel in H_2SO_4 solution

The values of Ea, ΔH_a, and ΔS_a obtained from Arrhenius plot were given in **Table 4**. At high concentrations (800 ppm and 1000 ppm), the calculated E_a values were greater than those for the blank ($E_{a,inh} > E_{a,blank}$). This increase in the energy barrier indicates that the metal dissolution rate is inhibited by the formation of a physical adsorption layer (physisorption), which tends to desorb as kinetic energy increases due to rising temperature. Furthermore, a physical adsorption process is further supported by the inhibitor efficiency of the steel is lower at high temperature [61]. The positive value of ΔH_a indicates the endothermic behaviour of metal dissolution alongside with higher value at high concentration as well. The higher and ΔH_a values mean the corrosion process requires more thermal energy to proceed when the inhibitor is added [62]. The negative value of entropy activation energy (ΔS_a) represents that the reactants (inhibitor molecules and metal surface ions) form an activated complex that is more organized or structured than the individual reactants moving freely in solution [63].

Table 4. Activation parameters for corrosion inhibitor of A. Muricata extract

Concentration	E_a (kJ mol^{-1})	ΔH_a (kJ mol^{-1})	ΔS_a (J mol^{-1} K^{-1})
Blank	81.93	79.30	-15.238
300 ppm	75.18	72.55	-10.944
500 ppm	78.65	76.02	-4.333
800 ppm	100.74	98.11	-61.121
1000 ppm	88.43	85.80	-16.880

3.3 Adsorption Isotherm

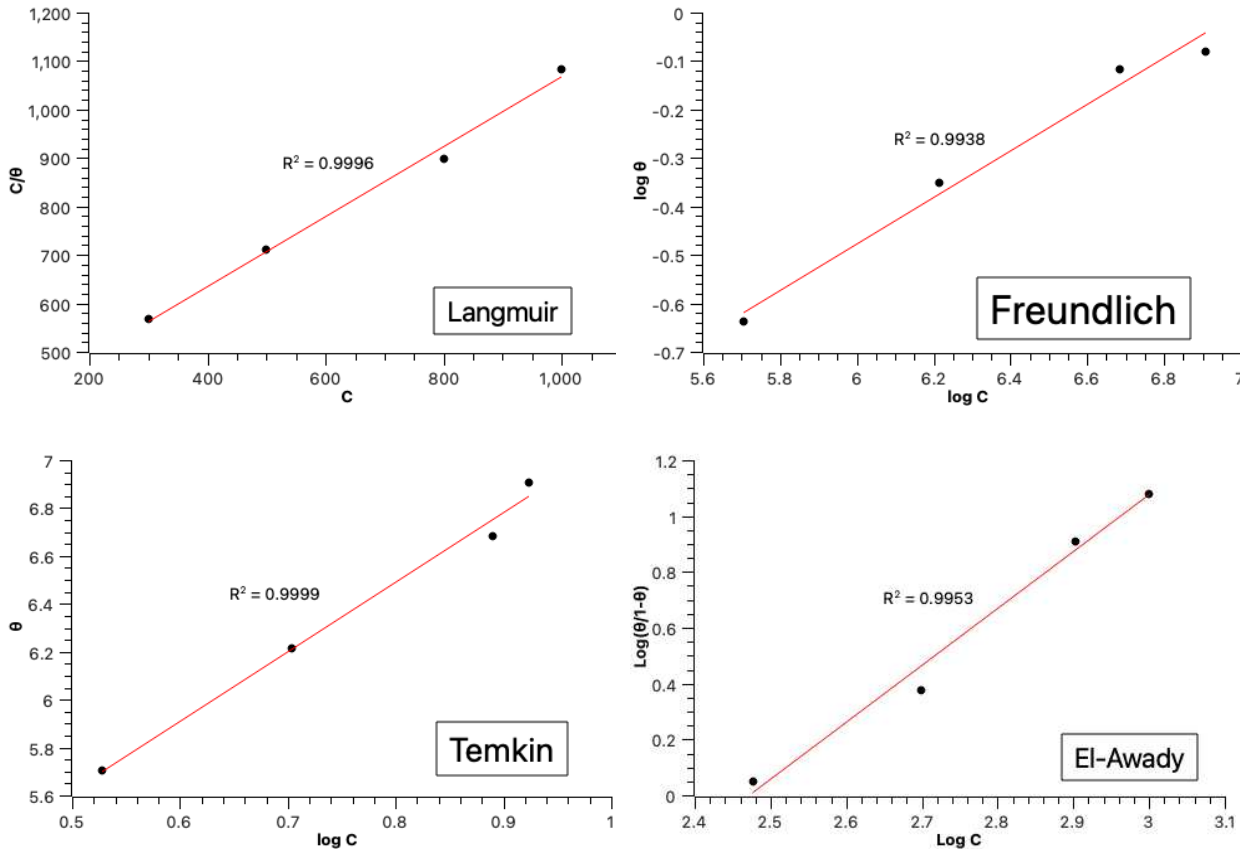

Figure 8. Adsorption isotherm plot of A. Muricata extracts on API 5L steel in H2SO4 solution using (a) Langmuir, (b) Freundlich, (c) Temkin, and (d) El-Awady

The understanding of inhibition mechanism of inhibitor molecule onto metal surfaces was important to explaining this phenomenon. The adsorption behaviour of A. muricata extract on API 5L steel in H_2SO_4 environment can be elaborated from EIS measurement data using several adsorption isotherm equations, such as Langmuir, Freundlich, Temkin, and El-Awady. However, the best linear fit is using Langmuir equation, which is shown in eq.5

$$\frac{C}{\theta} = \frac{1}{K_{ads}} + C \quad (4)$$

Where C represents concentration of inhibitor added, θ is surface coverage which obtained from EIS data, and K_{ads} is equilibrium constant. By plotting C vs C/θ (**Figure 8**), the slope and y-intersect data were obtained and the R^2 shows better fit with 0.999 which confirms that the adsorption inhibition of *A. muricata* extract follows Langmuir model equation. K_{ads} obtained from linear regression can be used to calculate the Gibbs free energy (ΔG^0_{ads}) which derived from eq.6

$$\Delta G^0_{ads} = -RTln(K_{ads}) \quad (5)$$

Where R is universal gas constant and T is temperature.

According to several literature, when ΔG^0_{ads} value was around -20 kJ/mol or lower, it indicates that the type of adsorption was physisorption. This type of adsorption involves electrostatic interactions between charged molecules and the charged metal surface. On the other hand, if ΔG^0_{ads} value around -40 kJ/mol or higher, it suggests that chemisorption was taken place. Which is defined by charge transfer or sharing from the inhibitor molecules to the metal surface, creating a coordinate bond [64,65]. In this study, the ΔG^0_{ads} value of A. muricata extract was -35.62 kJ/mol, suggesting the spontaneous and strong adsorption of inhibitor molecule onto the metal surface. The results also supported the literature, which is in between -20 kJ/mol and -40 kJ/mol suggesting the type of inhibition is mixed-type adsorption mechanism by combining both physisorption and chemisorption mechanism [66].

3.4 Surface Characterization

3.4.1 Scanning Electron Microscope (SEM) and Atomic Force Microscope (AFM)

Surface analysis of the polished steel, uninhibited steel and inhibited steel at 1000 ppm after 72 hours immersion in 1M H_2SO_4 solution was characterized using SEM and AFM, which is

shown in **Figure 9**. The polished steel shows a very smooth surface without any corrosion product detected from EDS spectra. In contrast, the uninhibited steel shows that the surface is severely corroded, leading to the production of numerous corrosion pits because of the very high steel dissolution. However, in the presence of *A. muricata* extract at 1000 ppm shows a contrast effect on the steel surface, giving a minimal impact and smoother surface compared to the uninhibited steel.

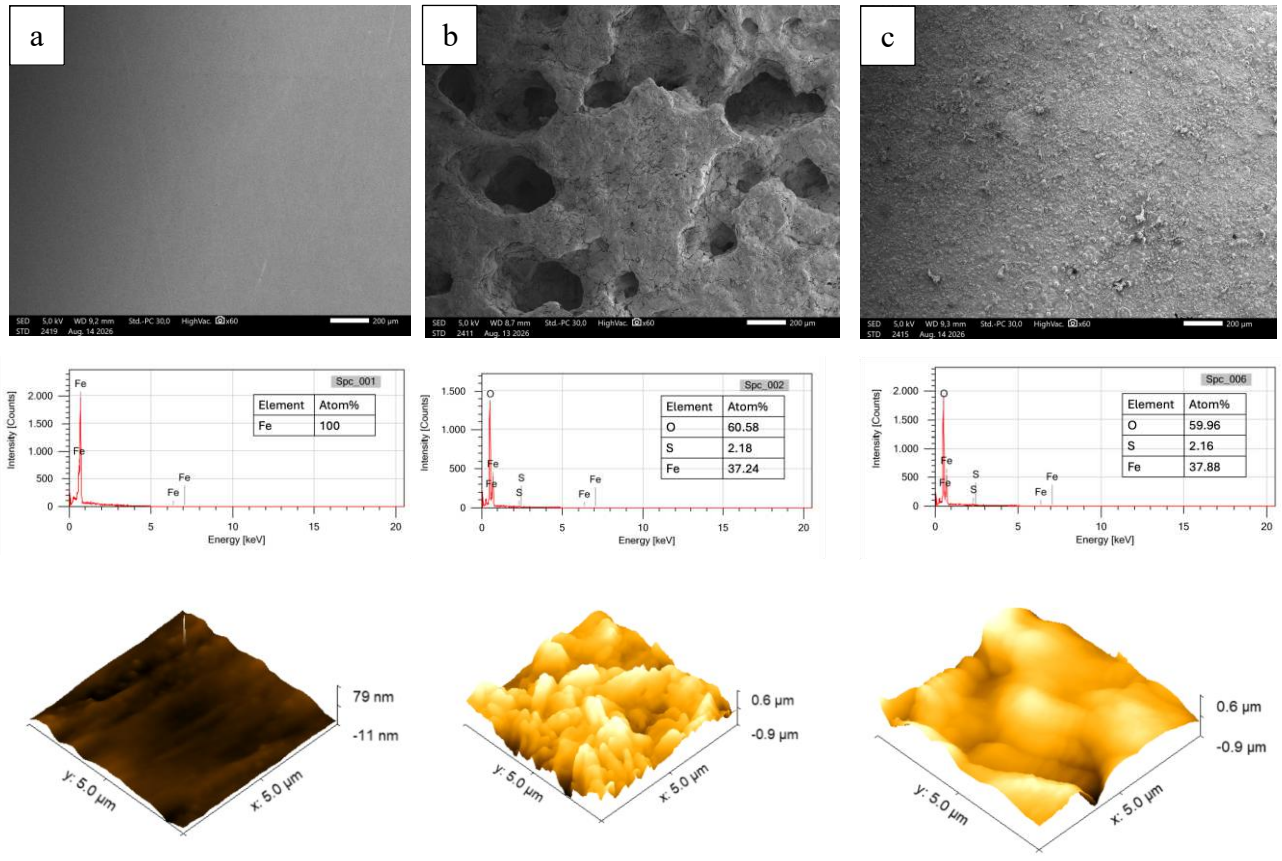

Figure 9. SEM EDX and AFM analysis of polished sample (a) uninhibited steel (b), and inhibited steel (c) at 1000 ppm in H_2SO_4 solution for 72 h.

This is also supported by the results of the 3D AFM analysis which confirms that the metal's surface in the presence of *A. muricata* extract has a smoother surface with roughness average 17.73 nm compared to the uninhibited steel with roughness average 60.74 nm. A smoother surface of API 5L steel indicates the formation of a protective film adhering to the steel surface and acts as a barrier against aggressive ions [67,68]. Additionally, the elemental composition detected from EDS spectra confirms a slight decrease of oxygen (O) and carbon (C) in the steel immersed with *A. Muricata* extract.

3.4.2 X-ray Photoelectron Spectroscopy (XPS)

The elemental compositions of the corrosion product film, or adsorption film, were analyzed using the XPS technique to gain a better understanding of whether the active chemicals were adsorbed onto the steel surface. Binding energy determined the element's valence states and current forms, and the peak area was used to calculate the relative atomic content. The *A. muricata*

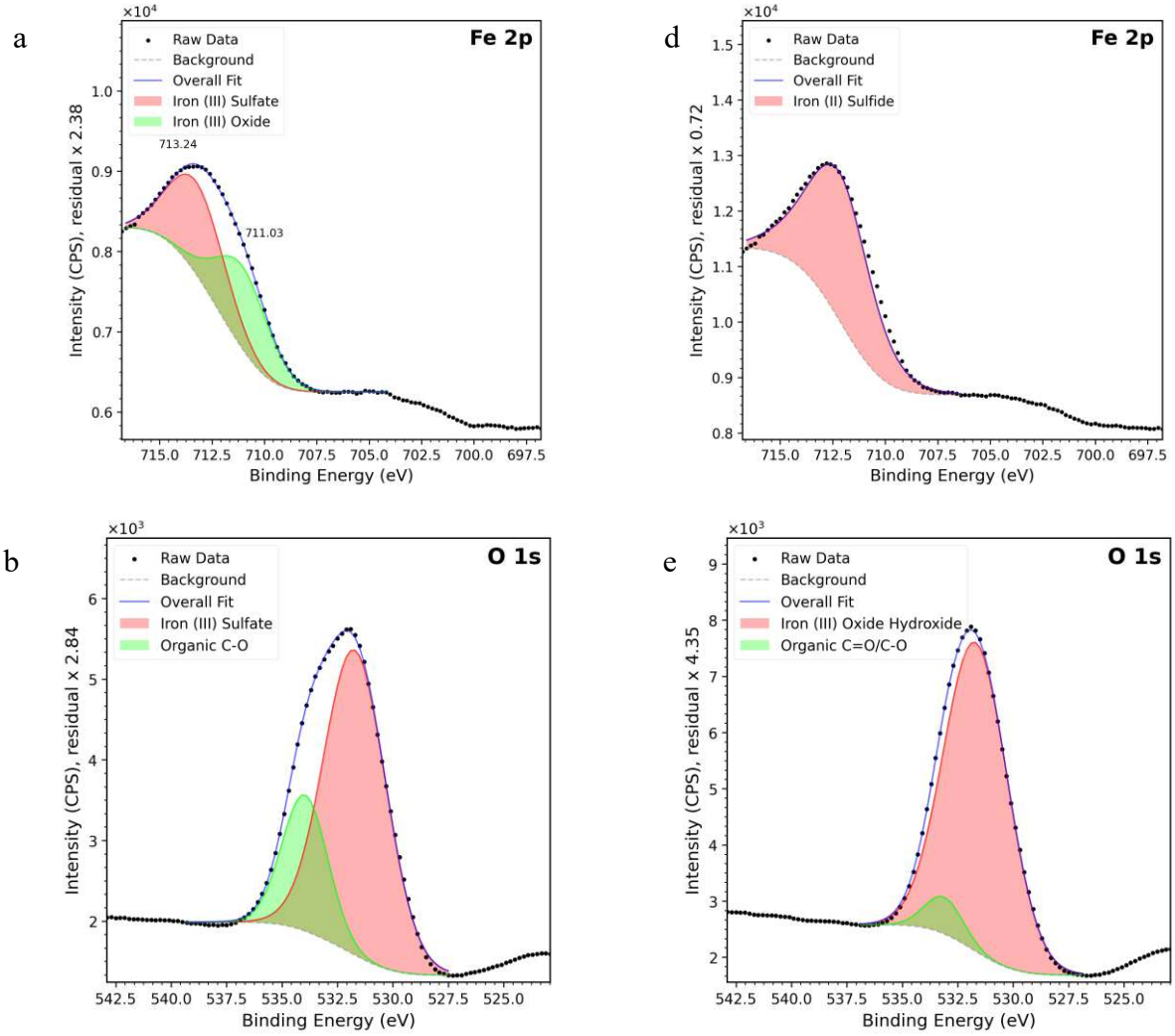

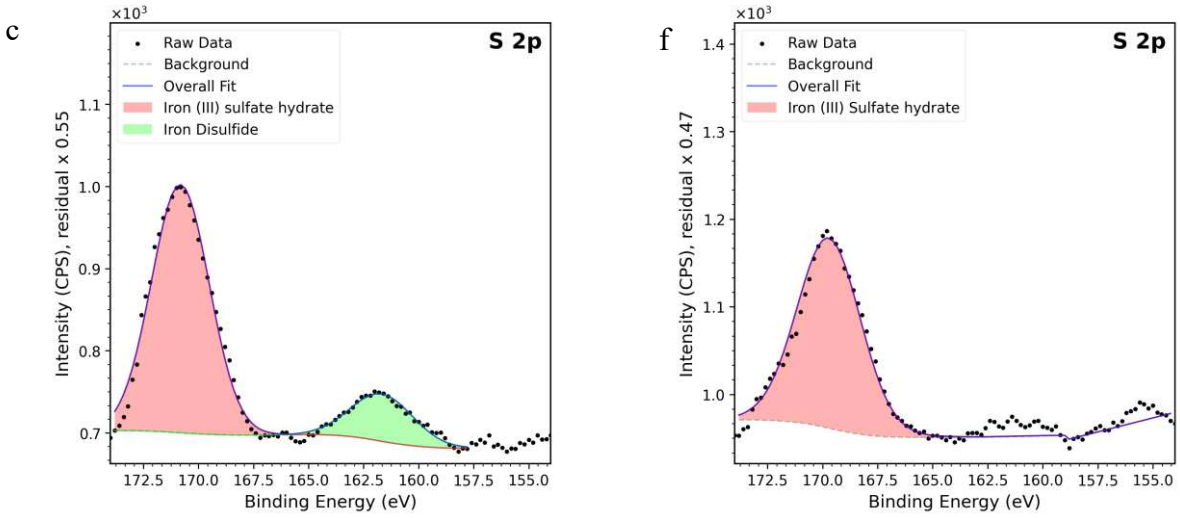

Figure 10. XPS Analysis of uninhibited steel (a,b,c) and inhibited steel at 1000 pm (d,e,f).

extract adsorption film on the steel's surface high resolution of Fe 2p3/2, O 1s, and S 2p were shown in **Error! Reference source not found.**.

In the blank sample with Fe2p resolution, there is peak that appears at 713.24 eV and 711.03 which confirms as $Fe_2(SO_4)_3$ and Fe_2O_3 (**Error! Reference source not found.**a). On the other hand, steel with addition of inhibitor (**Error! Reference source not found.**d) shows peak at 712.16 eV which confirms as $FeSO_4$ [69]. It suggests that the surface of the steel formed a corrosion product as a result of carbon steel that reacts with environments containing sulfuric acid (H_2SO_4) or sulphate ions. $FeSO_4$ found in inhibited steel was formed because of the steel reacts with dilute sulfuric acid or acidic sulphate-rich solutions through anodic dissolution ($Fe + H_2SO_4 \rightarrow FeSO_4 + H_2$) and acts as a primary salt layer on the metal surface [70]. Unlike inhibited steel, in the uninhibited steel was found $Fe_2(SO_4)_3$ and Fe_2O_3 which is formed via the further oxidation of ferrous ions or through the chemical reaction of ferric oxides or rust with sulfuric acid environments ($Fe_2O_3 + 3H_2SO_4 \rightarrow Fe_2(SO_4)_3 + 3H_2O$) [71].

In the XPS analysis of O1s for blank steel shows peak at 531.71 eV and 533.96 eV which is confirmed as $Fe_2(SO_4)_3$ and lattice oxygen (O^{2-}) corresponding to iron oxides like Fe_3O_4 [72]. In the presence of A. muricata extract, the XPS analysis shows peak at 531.68 eV and 533.12 eV which are associated as FeO(OH) and oxygen double bond of C=O, respectively. The double bond of C=O was found may be due to the adsorption of inhibitor molecules that occur on the metal surface [73,74].

The S2p XPS results of uninhibited steel shows there are two peaks at 170.82 eV and 161.66 eV, which associated as $Fe_2(SO_4)_3.xH_2O$ and FeS_2, respectively. Meanwhile, inhibited steel shows one peak at 169.72 which is also confirms as $Fe_2(SO_4)_3.xH_2O$. The formation of FeS_2 on uninhibited steel is caused by the steel surface being exposed to a corrosive environment containing Sulphur and lacking inhibitors [75,76].

3.5 DFT Analysis

Molecular studies of organic inhibitors were simulated based on DFT calculations which seem accurate to examine the adsorption behaviour of the active compounds in *A. muricata* extract on the surface of the steel and investigate the corrosion inhibition mechanism of the inhibitors. The DFT calculations performed using ORCA quantum chemistry software and visualized using Avogadro 2.0, employing B3LYP functional and 6-311++G (d, p) basis unit cell. The various energy quantum parameters were calculated, including HOMO energy (E_{HOMO}), LUMO energy (E_{LUMO}), the energy band gap (ΔE), the ionization potential (I), electron affinity (A), global hardness (ξ), and electronegativity (χ) which were used to calculate the electron capability to transfer from organic molecules to the metal surfaces (ΔN). The calculations to determine all those parameters were using the following equations [77–79]

$$\Delta E = E_{LUMO} - E_{HOMO} \quad (6)$$

$$I = -E_{HOMO} \quad (7)$$

$$A = -E_{LUMO} \quad (8)$$

$$\chi = \frac{I + A}{2} \quad (9)$$

$$\xi = \frac{I - A}{2} \quad (10)$$

$$\Delta N = \frac{\emptyset - \chi_{inhb}}{2\xi_{inhb}} \quad (11)$$

Figure 11 shows the van der Walls surface of major organic molecules, HOMO, and LUMO which found in *A. muricata* extract. The energy activity parameters which were obtained from DFT simulations were shown in Table 5.

The HOMO of m-Guaiacol was distributed uniformly throughout the benzene ring system as well as in the oxygen atoms of the methoxy ($-OCH_3$) and hydroxyl (-OH) groups. The lone pair

of electrons on the oxygen heteroatom strongly resonates with the aromatic π electron cloud, making it an active center for electron donation to the metal surface. The LUMO distributions are still highly concentrated on the aromatic ring. This allows the molecule to accept free electron density from the metal surface through feedback interaction. Because the HOMO and LUMO cover almost the entire surface of the flat ring, these molecules tend to adsorb in a parallel (flat) orientation on the steel surface, providing effective surface coverage.

In hexadecanoic acid, the electron density is localized exclusively in the carboxyl head group (-COOH), particularly at the carbonyl and hydroxyl oxygen atoms. It is also evident that the long aliphatic hydrocarbon chain does not contribute to the HOMO orbital. Similar to the HOMO distribution, the LUMO distribution is also confined to the C=O bond in the carboxyl group. This indicates that the -COOH group acts as a polar anchor that adheres perpendicular to the steel surface.

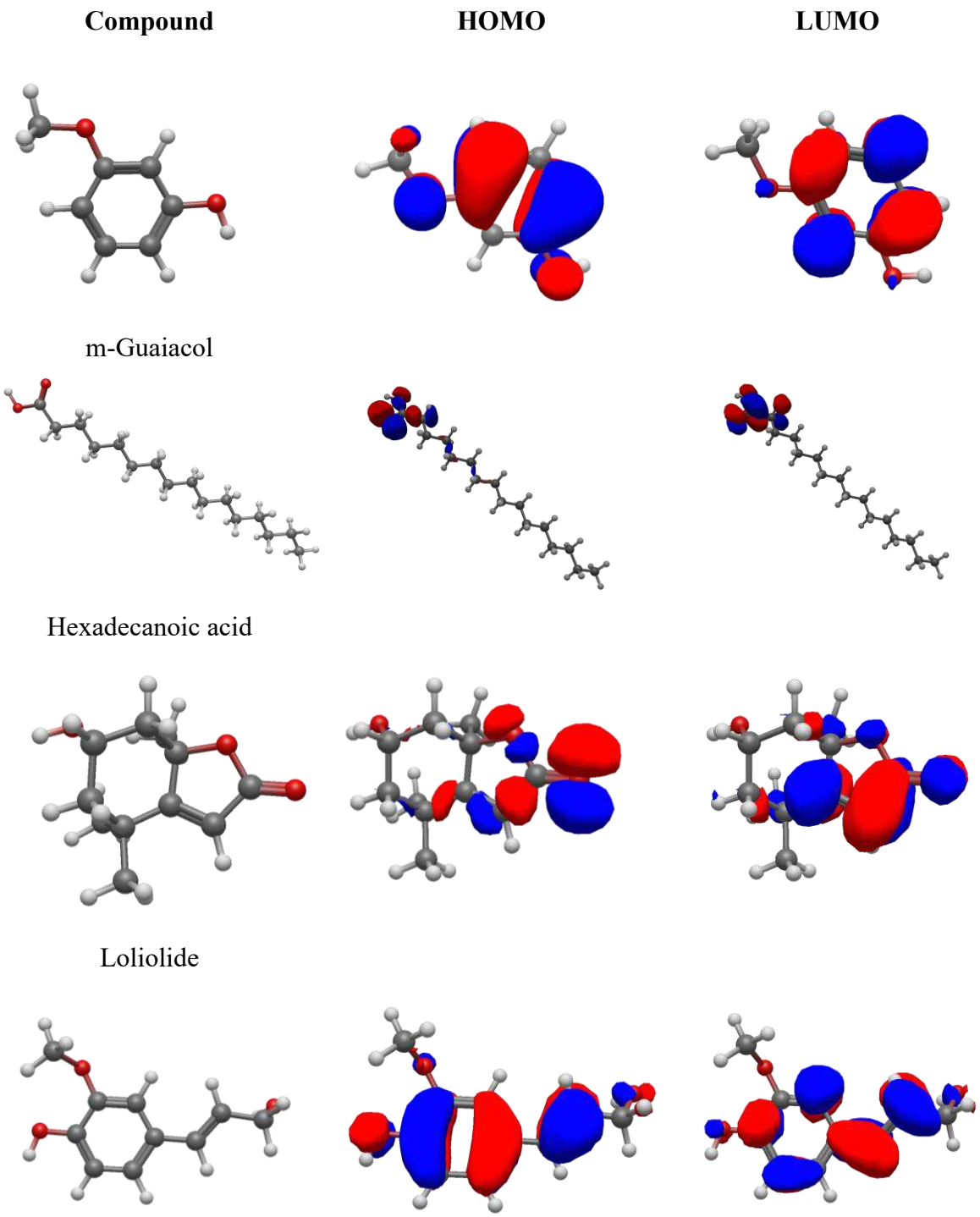

Figure 11. The structure, HOMO, and LUMO of major constituents in *A. Muricata* extract.

The HUMO and LUMO distribution of Loliolide also is concentrated in the heterocyclic ring, particularly around the C=C double bond and the lactone carbonyl group (C=O). Thus, it can

be said that the unsaturated lactone heterocyclic group acts as the primary active site in the electron donor-acceptor interaction with the iron substrate.

In 4-((1E)-3-Hydroxy-1-propenyl)-2-methoxyphenol, the electron density of the delocalized HOMO and LUMO is distributed uniformly across the entire benzene ring and extends to the aliphatic double bond (C=C) in the propenyl side chain. Because the HOMO and LUMO orbitals extend flat from the ends of the aromatic ring to the propenyl double bond, this molecule tends to attach horizontally/parallel (planar) to the steel surface, providing better coverage surface on the metal surface.

Table 5. Energy activity parameters of the major compounds in *A. Muricata* extract

Compound	E_{HOMO} (eV)	E_{LUMO} (eV)	ΔE (eV)	I (eV)	A (eV)	χ (eV)	ξ (eV)	ΔN (eV)
m-Guaiacol	-5.27	-0.99	4.27	5.27	0.99	3.13	2.14	0.91
Hexadecanoic acid	-8.04	0.33	8.36	8.04	-0.33	3.85	4.18	0.38
Loliolide	-7.58	-0.99	6.59	7.58	0.99	4.28	3.30	0.41
4-((1E)-3-Hydroxy-1-propenyl)-2-methoxyphenol	-6.07	-0.95	5.12	6.07	0.95	3.51	2.56	0.68

The energy activity parameters of each molecule were compared as shown in **Table 5**. A lower HOMO-LUMO energy gap in a corrosion inhibitor means that the molecule has high chemical reactivity but low electronic stability. Molecules with a low energy gap generally adsorb more easily and more firmly to metal surfaces, which inhibits the rate of corrosion [80]. From four major compounds in A. muricata extract, m-Guaiacol and 4-((1E)-3-Hydroxy-1-propenyl)-2-methoxyphenol has the smallest band gap energy with 4.27 eV and 5.12 eV, respectively. Therefore, m-Guaiacol and 4-((1E)-3-Hydroxy-1-propenyl)-2-methoxyphenol has the most active chemical reaction and gives excellent protection against H_2SO_4 for mild steel [81]. The global hardness (ξ) of m-Guaiacol is also the smallest which has the softest molecules that are highly sensitive to changes in electrons and readily donate their electrons to the metal surface [82]. Furthermore, the ΔN of all four major compounds is smaller than 3.6 eV suggesting that these molecules have exceptional capacities for electron donation and corrosion inhibition. m-Guaiacol and 4-((1E)-3-Hydroxy-1-propenyl)-2-methoxyphenol has the highest value of ΔN which results in a higher electron-donating capacity [82].

3.6 Mechanism of Inhibition

The inhibition mechanism of *A. muricata* extract was illustrated in **Figure 12**. The inhibition mechanism of plant extract primarily depends on chemical or physical adsorption of the compounds on metal surface. The Langmuir model explains that A. muricata extract occurs through physisorption and chemisorption. And from DFT studies, m-Guaiacol plays an important role as organic molecules that adsorb onto the metal surface due to small band gap energy and

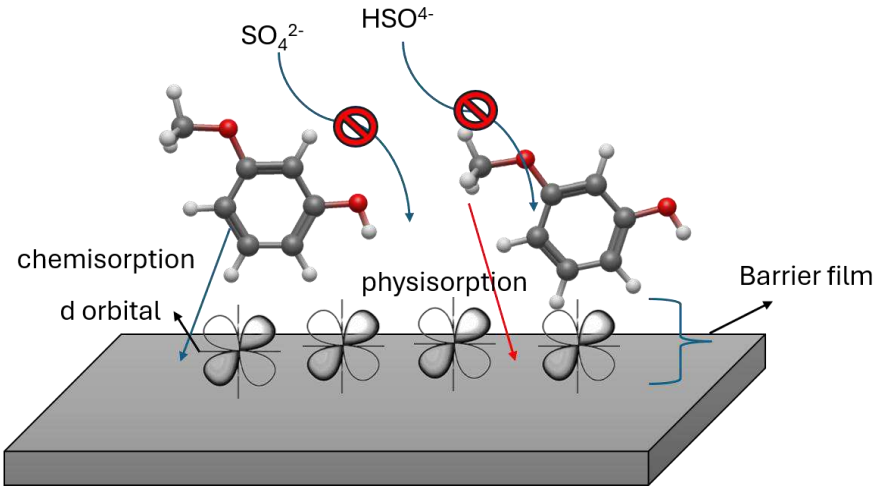

Figure 12. Schematic diagram inhibition mechanism of A. muricata extract on mild steel in H_2SO_4 environment

adsorb flat on the surface tends to have higher surface coverage. The electron donation of A. muricata extract with d-orbital of Fe is also relatively high, making it easier to replace the sulfate ions and water molecules which should be adsorbed onto the steel surface. As illustrated in **Figure 12**, the organic molecules create a barrier that inhibits the metal surface from corrosive ions such as HSO^{4-} and SO_4^{2-}, thus preventing the dissolution of metal. The formation of the protective inhibition films on the metal surface followed by multiple results such as lower corrosion rate, higher R_{ct} values, lower C_{dl}, and improved inhibition efficiency. In contrast, the corrosion reaction still occurs on the metal surface without inhibitor. Hence, *A. muricata* extract is a corrosion inhibitor that has been proven to be effective for steel and can protect steel surfaces with good coverage.

4. Conclusion

A. muricata leaf extract has proven to effectively mitigate corrosion rate of API 5L steel in aggressive sulfuric acid environment by forming a stable protective thin film. UV-Vis and FTIR characterization confirms the presence of electron-donating groups, such as aromatic conjugated

π systems as well as O and N heteroatoms from flavonoids, alkaloids, and tannins. Loliolide, hexadecanioc acid, m-Guaiacol, and 4-((1E)-3-Hydroxy-1-propenyl)-2-methoxyphenol was conformed as the major compounds found in the extract. The HOMO and LUMO profiles activity of the compounds distributions shows outstanding ability to adsorb onto the metal surface by facilitate electron donation to the d orbitals of Fe atoms. The success of the inhibitor adsorption was validated by a decrease in corrosion rate and increase efficiency inhibition up to 91% at 1000 ppm. The adsorption mechanism of molecular inhibitors follows the Langmuir isothermal equation, and the study shows that the inhibitors are adsorbed onto the metal surface via physisorption and chemisorption. The SEM observations confirmed that the inhibitor successfully protected the steel surface from corrosion; compared to the steel treated with the inhibitor, the steel surface without the inhibitor showed numerous corrosion pits. The XPS results also confirm that the active components of *A. muricata* extract play a role in protecting the steel surface, as no damaging corrosion products were found during the corrosion process.

Acknowledgment

This study was supported by seed funding from University of Indonesia with grant number PKS-3694/UN2.F4.D/PPM.00.00/2025; research facility form National Research and Innovation Agency, Republic of Indonesia; and scholarship funding from Indonesia Endowment Fund for Education, Ministry of Finance, Republic of Indonesia.

Data Availability

The datasets generated and analyzed during the current study are available from the corresponding author upon reasonable request.

Reference

[1] Sulzer Pumps, Materials and Corrosion, Centrifugal Pump Handbook (2010) 227–250. https://doi.org/10.1016/B978-0-7506-8612-9.00008-5.

[2] G. Koch, Cost of corrosion, Trends in Oil and Gas Corrosion Research and Technologies: Production and Transmission (2017) 3–30. https://doi.org/10.1016/B978-0-08-101105-8.00001-2.

[3] G. Terán Méndez, S.I. Capula-Colindres, J.C. Velázquez, D. Angeles-Herrera, N.E. González-Arévalo, E. Torres-Santillan, A. Cervantes-Tobón, Mechanical Characterization of Resistance-Welded and Seamless API 5L X52 Pipes: A Comparative Study, Coatings 2024, Vol. 14, Page 343 14 (2024) 343. https://doi.org/10.3390/COATINGS14030343.

[4] S. Nazar, S. Lipiec, E. Proverbio, FEM modelling of hydrogen embrittlement in API 5L X65 steel for safe hydrogen transportation, Journal of Materials Science: Materials in Engineering 20 (2025) 9-. https://doi.org/10.1186/S40712-025-00221-Y/FIGURES/8.

[5] M.C. De Oliveira, R.M. Figueredo, H.A. Acciari, E.N. Codaro, Corrosion behavior of API 5L X65 steel subject to plastic deformation, Journal of Materials Research and Technology 7 (2018) 314–318. https://doi.org/10.1016/J.JMRT.2018.02.006.

[6] Mujiono, F. Mubarok, Failure Analysis of API 5L Grade B Underground Crude Oil Transfer Pipe, Engineering Proceedings 2024, Vol. 63, Page 29 63 (2024) 29. https://doi.org/10.3390/ENGPROC2024063029.

[7] A. Bahadori, Surface Preparation for Coating, Painting, and Lining, Essentials of Coating, Painting, and Lining for the Oil, Gas and Petrochemical Industries (2015) 1–105. https://doi.org/10.1016/B978-0-12-801407-3.00001-8.

[8] Woodard & Curran, Inc., Wastes from Industries (Case Studies), in: Industrial Waste Treatment Handbook, Elsevier, 2006: pp. 409–496. https://doi.org/10.1016/B978-075067963-3/50012-6.

[9] R. Aslam, M. Mobin, S. Zehra, J. Aslam, A comprehensive review of corrosion inhibitors employed to mitigate stainless steel corrosion in different environments, J. Mol. Liq. 364 (2022) 119992. https://doi.org/10.1016/J.MOLLIQ.2022.119992.

[10] J.A. Richardson, Corrosion in Sulfuric Acid, in: Shreir's Corrosion, Elsevier, 2010: pp. 1226–1249. https://doi.org/10.1016/B978-044452787-5.00180-3.

[11] N. Hossain, M. Aminul Islam, M. Asaduzzaman Chowdhury, Advances of plant-extracted inhibitors in metal corrosion reduction – Future prospects and challenges, Results Chem. 5 (2023). https://doi.org/10.1016/j.rechem.2023.100883.

[12] Z. Ghehsareh, T. Sayah, M. Moharramnejad, A. Rahimitabar, A. Ehsani, Green guardians: A comprehensive review of environmentally friendly corrosion inhibitors from plant extract to ionic-liquids in industrial applications, Prog. Org. Coat. 201 (2025). https://doi.org/10.1016/j.porgcoat.2025.109146.

[13] M.E. Eissa, S.H. Etaiw, E.S. El-Hussieny, A.A. El-Hossiany, A.E.A.S. Fouda, Sweet Orange Peel Extract as green sustainable corrosion inhibitor for Al in 1 M HCl, International Journal of Electrochemical Science 20 (2025). https://doi.org/10.1016/j.ijoes.2024.100882.

[14] I.C. Amarachukwu, C. Vitalis Ikenna, J. Abosede, A. Onyewuchi, Green Metal Protection: Optimizing the Efficiency of Ethanolic Extracts of Lagenaria Breviflora Leaf as Corrosion Inhibitor for Mild Steel Dissolution in 0.5M HCl Medium, Results in Engineering (2025) 107754. https://doi.org/10.1016/j.rineng.2025.107754.

[15] M.A. Ahmed, S. Amin, A.A. Mohamed, Current and emerging trends of inorganic, organic and eco-friendly corrosion inhibitors, RSC Adv. 14 (2024) 31877–31920. https://doi.org/10.1039/D4RA05662K.

[16] N. Kumar, P. Anunay, S. Kumar, L.K. Meena, D. Singh, An overview on emerging green organic corrosion inhibitors: sustainable solution for oil and gas industrial applications, RSC Adv. 16 (2026) 3909. https://doi.org/10.1039/D5RA08166A.

[17] N.S. Phadke, Seranthimata Samshuddin, Assessment of Neem Tree Extracts as Corrosion Inhibitors: An Overview, Surface Engineering and Applied Electrochemistry 62 (2026) 167–177. https://doi.org/10.3103/S1068375526700080/TABLES/2.

[18] A. Sihmar, N. Dua, H. Assad, R. Kumar, H. Kumar, H. Dahiya, Unveiling the corrosion mitigation of mild steel by green inhibitor derived from OperculinaTurpethum Roots Extract (OTE): A comprehensive electrochemical, surface and computational insights, J. Mol. Struct. 1381 (2027) 147754. https://doi.org/10.1016/J.MOLSTRUC.2026.147754.

[19] Z. Tang, P. Wang, Y. Song, W. Liu, K.R. Ansari, A. Singh, Y. Lin, Study on the synergistic corrosion inhibition effect of metal ion modified citrus peel extract on Q235 carbon steel in hydrochloric acid, Journal of the Indian Chemical Society 102 (2025). https://doi.org/10.1016/j.jics.2025.102172.

[20] L.B. Furtado, R.C.G. da Silva, W.F. de Oliveira, M.J.O.C. Guimarães, G.B. Leoni, E.C.A.N. Chrisman, L.J. de Carvalho, S.L.D.C. Brasil, J.A. da C.P. Gomes, Phenolic compounds as eco-friendly corrosion inhibitor obtained by optimized extraction from residual broccoli leaves, Results Chem. 17 (2025) 102562. https://doi.org/10.1016/J.RECHEM.2025.102562.

[21] A. El Ouaddari, R. Kellal, Z. Ait El Caid, R. Albarakati, N. Wazzan, O.S. Al-Qurashi, Z. Safi, S. Iben Moussa, A. El Amrani, M. Zertoubi, D. Benmessaoud Left, Insight into anti-

corrosion behavior of Cladanthus mixtus (L.) flower extracts as a biodegradable inhibitor for carbon steel in acid medium: Experimental and theoretical studies, Mater. Chem. Phys. 326 (2024) 129827. https://doi.org/10.1016/J.MATCHEMPHYS.2024.129827.

[22] O. Belhadj, Z. El Fakir, A. El Amri, A. Idrissi, C. Sghir, S. Bouzakraoui, M. Ouakki, M. Cherkaoui, Black Mustard Seed Extract as a new greener corrosion inhibitor: Experimental and DFT studies, Colloids Surf. A Physicochem. Eng. Asp. 707 (2025). https://doi.org/10.1016/j.colsurfa.2024.135911.

[23] G. Doumane, J. Bensalah, M. Ouakki, Z. Aribou, O. Boussalem, K. Mzioud, Z.S. Safi, A. Berisha, M. Bourhia, A.R. Z. Gaafar, S. Ibenmoussa, G.F. Wondmie, A. Zarrouk, M.E. Touhami, A. Habsaoui, Alkaloid extract of seed Citrullus colocynthis as novel green inhibitor for mild steel corrosion in one molar HCl acid solution: DFT and MC/MD approaches, Sci. Rep. 14 (2024). https://doi.org/10.1038/s41598-024-67011-y.

[24] K.D.H. Nguyen, T.D. Manh, L.T.P. Nguyen, D.T. Vu, K.L. Duong Ngo, Syzygium polyanthum (Wight) Walp. leaf extract as a sustainable corrosion inhibitor for carbon steel in hydrochloric acidic environment, Journal of Industrial and Engineering Chemistry 143 (2025) 468–487. https://doi.org/10.1016/J.JIEC.2024.08.054.

[25] M. Jokar, T.S. Farahani, B. Ramezanzadeh, Electrochemical and surface characterizations of morus alba pendula leaves extract (MAPLE) as a green corrosion inhibitor for steel in 1 M HCl, J. Taiwan Inst. Chem. Eng. 63 (2016) 436–452. https://doi.org/10.1016/J.JTICE.2016.02.027.

[26] Moch.B. Bahtiar, Sulistijono, L. Noerochim, T.N. Rohmannudin, B.A. Kurniawan, R.K. Pramadewandaru, Improved corrosion behaviour of A36 carbon steel in 3.5% NaCl solution via bio-inhibitor of mangkok leaf extract (Polyscias Scutellaria), Results in Engineering 29 (2026) 109412. https://doi.org/10.1016/J.RINENG.2026.109412.

[27] Y. Feng, B. Zhou, M. Wang, K. Xu, X. Geng, Z. Zuo, Y. Cao, G. Tian, Q. Li, J. Liao, Synergistic adsorption mechanism of pulsatilla chinensis root extract as an eco-friendly corrosion inhibitor for carbon steel in acidic solution, Environ. Res. 285 (2025) 122645. https://doi.org/10.1016/J.ENVRES.2025.122645.

[28] A.K. Nunach, G. Rani, R. Ahlawat, Corrosion Inhibition Potential of Cymbopogon citratus (Lemongrass) Leaves Extract on Mild Steel in 0.1 M Sulphuric Acid Medium at Different

Temperatures, Asian Journal of Chemistry 35 (2023) 1810–1818. https://doi.org/10.14233/ajchem.2023.27966.

[29] D.R. Gusti, R.D. Puspitasari, Harizon, J. Pebralia, I. Lestari, R. Restu Luky Anggara, I.A. Wulandari, M.A. Daya, Imelda, Eco-friendly corrosion inhibitors (combination of Macaranga gigantea sap extract and maltodextrin) on mild steel in sulfuric acid media, Results in Surfaces and Interfaces 23 (2026) 100762. https://doi.org/10.1016/J.RSURFI.2026.100762.

[30] A. V. Coria-Téllez, E. Montalvo-Gónzalez, E.M. Yahia, E.N. Obledo-Vázquez, Annona muricata: A comprehensive review on its traditional medicinal uses, phytochemicals, pharmacological activities, mechanisms of action and toxicity, Arabian Journal of Chemistry 11 (2018) 662–691. https://doi.org/10.1016/J.ARABJC.2016.01.004.

[31] S. Fofana, R. Ziyaev, A. Abdusamatov, S.K. Zakirov, Alkaloids from Annona muricata leaves, Chemistry of Natural Compounds 2011 47:2 47 (2011) 321–321. https://doi.org/10.1007/S10600-011-9921-5.

[32] A.S. Nugraha, R. Haritakun, J.M. Lambert, C.T. Dillon, P.A. Keller, Alkaloids from the root of Indonesian Annona muricata L, Nat. Prod. Res. 35 (2019) 481–489. https://doi.org/10.1080/14786419.2019.1638380.

[33] S. Mohanty, J. Hollinshead, L. Jones, P.W. Jones, D. Thomas, A.A. Watson, D.G. Watson, A.I. Gray, R.J. Molyneuxc, R.J. Nash, Annona muricata (Graviola): Toxic or therapeutic, Nat. Prod. Commun. 3 (2008) 31–33. https://doi.org/10.1177/1934578x0800300107.

[34] M. Nawwar, N. Ayoub, S. Hussein, A. Hashim, R. El-Sharawy, K. Wende, M. Harms, U. Lindequist, Flavonol triglycoside and investigation of the antioxidant and cell stimulating activities of Annona muricata Linn., Archives of Pharmacal Research 2012 35:5 35 (2012) 761–767. https://doi.org/10.1007/S12272-012-0501-4.

[35] J. Correa Gordillo, D. Ortiz, J.E. Larrahondo, M. Sánchez Mejía, H. Pachón, Soursop (Annona muricata L.) antioxidant activity: A literature review[Actividad antioxidante en guanábana (Annona muricata l.): Una revisión bibliográfica], Bol. Latinoam. Caribe Plantas Med. Aromat. 11 (2012) 111–126. https://www.scopus.com/pages/publications/84859032938 (accessed December 16, 2025).

[36] Y.I. Kuznetsov, G. V. Redkina, Thin Protective Coatings on Metals Formed by Organic Corrosion Inhibitors in Neutral Media, Coatings 2022, Vol. 12, Page 149 12 (2022) 149. https://doi.org/10.3390/COATINGS12020149.

[37] R. Karki, A.K. Bajgai, N. Khadka, O. Thapa, T. Mukhiya, H.B. Oli, D.P. Bhattarai, Acacia catechu Bark Alkaloids as Novel Green Inhibitors for Mild Steel Corrosion in a One Molar Sulphuric Acid Solution, Electrochem 3 (2022) 668–687. https://doi.org/10.3390/electrochem3040044.

[38] A. Matsushige, Y. Kotake, K. Matsunami, H. Otsuka, S. Ohta, Y. Takeda, Annonamine, a New Aporphine Alkaloid from the Leaves of Annona muricata, Chem. Pharm. Bull. (Tokyo). 60 (2012) 257–259. https://doi.org/10.1248/CPB.60.257.

[39] P. Shathani, E.N. Ogunmuyiwa, B.A. Obadele, O.P. Oladijo, Eco-friendly corrosion inhibition of API 5L X42 steel in acidic media using Sclerocarya birrea leaf extract: Experimental, thermodynamic and computational insights, Chemical Thermodynamics and Thermal Analysis 20 (2025) 100215. https://doi.org/10.1016/J.CTTA.2025.100215.

[40] K.Y. Hsiao, R.J. Chung, P.P. Chang, T.H. Tsai, Identification of Hydroxyl and Polysiloxane Compounds via Infrared Absorption Spectroscopy with Targeted Noise Analysis, Polymers 2025, Vol. 17, Page 1533 17 (2025) 1533. https://doi.org/10.3390/POLYM17111533.

[41] A.I. Obike, K.S. Eze, I. Abdel-Rahman, A.I. Ikeuba, I.K. Nwokolo, C. Aghalibe, Evaluation of Corynocarpus laevigatus extract as a green corrosion retardant for mild steel in acidic media: A combined gravimetric, gasometric and electrochemical methods, Current Research in Green and Sustainable Chemistry 10 (2025) 100447. https://doi.org/10.1016/J.CRGSC.2025.100447.

[42] N.A. Barghout, A. El Nemr, B.A. Abd-El-Nabey, H.A. Fetouh, S. Ragab, N.O. Eddy, Use of orange peel extract as an inhibitor of stainless steel corrosion during acid washing in a multistage flash desalination plant, J. Appl. Electrochem. 53 (2023) 379–399. https://doi.org/10.1007/S10800-022-01772-0/FIGURES/15.

[43] B. Ergel, R. Yıldız, S. Arslanhan, M.F. Baran, A new green corrosion inhibitor for mild steel in 1 M HCl using Erodium cicutarium (L.) leaf extract: Insights from both theoretical and experimental methods, Appl. Surf. Sci. 722 (2026) 165587. https://doi.org/10.1016/J.APSUSC.2025.165587.

[44] Z. Jiang, S. Deng, Y. Qiang, J. Xu, X. Li, Enhanced corrosion resistance of cold rolled steel in phosphoric acid solution with synergistic action of Camellia oleifera shell extract and 2-mercaptopyrimidine, J. Mol. Struct. 1345 (2025). https://doi.org/10.1016/j.molstruc.2025.143046.

[45] A. Cojocaru, G.E. Badea, I. Maior, S. Dzitac, O.D. Stănășel, M. Sebeșan, C.D. Ionaș, P. Creț, Electrochemical Investigations of Galium verum Ethanolic Extract as a Steel Corrosion Eco-Inhibitor in the Acid Media: An Unexpected Versatility of Plant Chemistry, Materials 18 (2025). https://doi.org/10.3390/ma18092078.

[46] A.J. Mwakalesi, Corrosion Inhibition of Mild Steel in Sulphuric Acid Solution with Tetradenia riparia Leaves Aqueous Extract: Kinetics and Thermodynamics, Biointerface Res. Appl. Chem. 13 (2023). https://doi.org/10.33263/BRIAC131.032.

[47] S.I. Ezugha, C.C. Aralu, Evaluation of adsorption and corrosion inhibition properties of Solanum Macrocarpon leaves extract on mild steel in sulphuric acid solutions, SN Appl. Sci. 5 (2023). https://doi.org/10.1007/s42452-023-05594-3.

[48] O. Olamide, A. David, A. Olanrewaju Seun, O.S. Bello, Optimization and inhibitive effects of Sweet Potato Leaf Extract (SPLE) on mild steel, Chemical Data Collections 45 (2023) 101015. https://doi.org/10.1016/J.CDC.2023.101015.

[49] N. Pham Van, N.C.T. Hoang, T.D. Manh, L.T. Dung, N.S. Hoai Vu, S. V. Prabhakar Vattikuti, C. Panaitescu, T.T. Pham, N. Nguyen Dang, Enhancing corrosion resistance of mild steel in hydrochloric acid with Chiquita banana sap extract, RSC Adv. 14 (2024) 14263–14277. https://doi.org/10.1039/d4ra00132j.

[50] V. Pinto, G.M. Pinto, L.D. Kateel, A. Thomas, Green Approach to Corrosion Inhibition of Mild Steel in Hydrochloric Acidusing Extractfromthe Pericarp of the fruit Tamarindus indica (Tamarind), Biointerface Res. Appl. Chem. 13 (2023). https://doi.org/10.33263/BRIAC136.544.

[51] J.P. Rajan, Corrosion Inhibition of Mild Steel in Hydrochloric Acid Solution using Methanolic Extracts of Elsholtzia communis and Spilanthes acmella as Green Inhibitors, Asian Journal of Chemistry 36 (2024) 2129–2138. https://doi.org/10.14233/ajchem.2024.32174.

[52] A.A. Sulaimon, P.I. Murungi, B.N. Tackie-Otoo, P.C. Nwankwo, M.A. Bustam, Analysis of natural okra extracts as corrosion inhibitors for mild steel in acidic medium, Environ. Sci. Pollut. Res. Int. 30 (2023) 119309–119328. https://doi.org/10.1007/s11356-023-30635-0.

[53] O. Belhadj, Z. El Fakir, A. El Amri, A. Idrissi, C. Sghir, S. Bouzakraoui, M. Ouakki, M. Cherkaoui, Black Mustard Seed Extract as a new greener corrosion inhibitor: Experimental and DFT studies, Colloids Surf. A Physicochem. Eng. Asp. 707 (2025). https://doi.org/10.1016/j.colsurfa.2024.135911.

[54] F. Gapsari, P.H. Setyarini, K. Anam, S. Hadisaputra, S. Hidayatullah, Purnami, A.M. Sulaiman, C.W. Lai, Efficacy of Andrographis paniculata leaf extract as a green corrosion inhibitor for mild steel in concentrated sulfuric acid: Experimental and computational insights, Results in Surfaces and Interfaces 18 (2025) 100361. https://doi.org/10.1016/J.RSURFI.2024.100361.

[55] S.A. Hussein, A.A. Khadom, Okra leaves extract as green corrosion inhibitor for steel in sulfuric acid: Gravimetric, electrochemical, and surface morphological investigations, Results Chem. 8 (2024). https://doi.org/10.1016/j.rechem.2024.101566.

[56] H. Kumar, P. Yadav, R. Kumari, R. Sharma, S. Sharma, D. Singh, H. Dahiya, P. Kumar, S. Bhardwaj, P. Kaur, Highly efficient green corrosion inhibitor for mild steel in sulfuric acid: Experimental and DFT approach, Colloids Surf. A Physicochem. Eng. Asp. 675 (2023). https://doi.org/10.1016/j.colsurfa.2023.132039.

[57] S. Aourabi, M. Driouch, M. Sfaira, F. Mahjoubi, B. Hammouti, C. Verma, E.E. Ebenso, L. Guo, Phenolic fraction of Ammi visnaga extract as environmentally friendly antioxidant and corrosion inhibitor for mild steel in acidic medium, J. Mol. Liq. 323 (2021) 114950. https://doi.org/10.1016/J.MOLLIQ.2020.114950.

[58] V. Konovalova, The effect of temperature on the corrosion rate of iron-carbon alloys, Mater. Today Proc. 38 (2021) 1326–1329. https://doi.org/10.1016/J.MATPR.2020.08.094.

[59] A. Kumar, C. Das, A novel eco-friendly inhibitor of chayote fruit extract for mild steel corrosion in 1 M HCl: Electrochemical, weight loss studies, and the effect of temperature, Sustain. Chem. Pharm. 36 (2023). https://doi.org/10.1016/j.scp.2023.101261.

[60] M. Pinelo, M. Rubilar, M. Jerez, J. Sineiro, M.J. Núñez, Effect of Solvent, Temperature, and Solvent-to-Solid Ratio on the Total Phenolic Content and Antiradical Activity of

Extracts from Different Components of Grape Pomace, J. Agric. Food Chem. 53 (2005) 2111–2117. https://doi.org/10.1021/JF0488110.

[61] M.M. Motawea, N.S. Al-Subaie, A.A.O. Younes, M.M.A.H. Shanab, Z.E. Ahmed, R.A. Abdelhadi, A.M. Abou Zeid, The adsorption behavior and inhibitive action of hydrocotyle umbellata leaf extract on corrosion of API5L L360 carbon steel in 0.5 M H2SO4 solution, BMC Chem. 20 (2026). https://doi.org/10.1186/s13065-026-01881-3.

[62] B.M. Prasanna, B.M. Praveen, N. Hebbar, T. V. Venkatesha, H.C. Tandon, Inhibition study of mild steel corrosion in 1 M hydrochloric acid solution by 2-chloro 3-formyl quinoline, International Journal of Industrial Chemistry 7 (2016) 9–19. https://doi.org/10.1007/S40090-015-0064-6/FIGURES/11.

[63] O.A. Akinbulumo, O.J. Odejobi, E.L. Odekanle, Thermodynamics and adsorption study of the corrosion inhibition of mild steel by Euphorbia heterophylla L. extract in 1.5 M HCl, Results in Materials 5 (2020). https://doi.org/10.1016/j.rinma.2020.100074.

[64] T.K. Sarkar, M. Yadav, I.B. Obot, Mechanistic evaluation of adsorption and corrosion inhibition capabilities of novel indoline compounds for oil well/tubing steel in 15% HCl, Chemical Engineering Journal 431 (2022) 133481. https://doi.org/10.1016/J.CEJ.2021.133481.

[65] N. G S, Kavyarathna, M. H N, R. K, N. Reddy, Green corrosion inhibition of mild steel using crude and successive extracts of Curcuma longa Linn. leaves, Next Research 10 (2026) 101833. https://doi.org/10.1016/J.NEXRES.2026.101833.

[66] E. Discover, S. Al-Amiery, A. Al-Amiery, L.M. Shaker, Green and hybrid corrosion inhibitors from adsorption mechanisms to deployable performance, Discover Electrochemistry 2026 3:1 3 (2026) 54-. https://doi.org/10.1007/S44373-026-00141-2.

[67] M.R. Rathod, S.K. Rajappa, R.L. Minagalavar, B.M. Praveen, B.K. Devendra, A.A. Kittur, Investigation of African mangosteen leaves extract as an environment-friendly inhibitor for low carbon steel in 0.5 M H2SO4, Inorg. Chem. Commun. 140 (2022) 109488. https://doi.org/10.1016/J.INOCHE.2022.109488.

[68] M. Alimohammadi, M. Ghaderi, A. Ramazani S.A, M. Mahdavian, Falcaria vulgaris leaves extract as an eco-friendly corrosion inhibitor for mild steel in hydrochloric acid media, Scientific Reports 2023 13:1 13 (2023) 3737-. https://doi.org/10.1038/s41598-023-30571-6.

[69] M.C. Biesinger, B.P. Payne, A.P. Grosvenor, L.W.M. Lau, A.R. Gerson, R.S.C. Smart, Resolving surface chemical states in XPS analysis of first row transition metals, oxides and hydroxides: Cr, Mn, Fe, Co and Ni, Appl. Surf. Sci. 257 (2011) 2717–2730. https://doi.org/10.1016/J.APSUSC.2010.10.051.

[70] B.Y. Wu, W. Liang, A.H. Wang, Compositional design of low carbon sulphuric acid dewpoint corrosion resistant steel and corresponding anticorrosive mechanism, Corrosion Engineering Science and Technology 48 (2013) 313–320. https://doi.org/10.1179/1743278212Y.0000000071;JOURNAL:JOURNAL:CESB;WEBSITE:WEBSITE:SAGE;WGROUP:STRING:PUBLICATION.

[71] Y.G. Avdeev, Y.I. Kuznetsov, Effect of iron(III) salts on steel corrosion in acid solutions. A review 1, Int. J. Corros. Scale Inhib 10 (2021) 1069–1109. https://doi.org/10.17675/2305-6894-2021-10-3-15.

[72] K. Subbiah, H.S. Lee, M.R. Al-Hadeethi, T. Park, H. Lgaz, Unraveling the anti-corrosion mechanisms of a novel hydrazone derivative on steel in contaminated concrete pore solutions: An integrated study, J. Adv. Res. 58 (2023) 211. https://doi.org/10.1016/J.JARE.2023.08.016.

[73] M. Honarvar Nazari, M.S. Shihab, E.A. Havens, X. Shi, Mechanism of corrosion protection in chloride solution by an apple-based green inhibitor: experimental and theoretical studies, Journal of Infrastructure Preservation and Resilience 1 (2020). https://doi.org/10.1186/s43065-020-00007-w.

[74] B. lan Lin, X. xin Zhou, T. hu Duan, C. Zhao, J. hao Zhu, Y. ye Xu, Experimental and theoretical study on corrosion inhibition and adsorption performance of Ipomoea batatas L. leaf extract for mild steel, Arabian Journal of Chemistry 17 (2024). https://doi.org/10.1016/j.arabjc.2023.105410.

[75] T. Van Nguyen, N.T.N. Truong, P. Ho, T.K. Trinh, J.H. Kim, C. Park, Green and simple preparation of carbon-coated iron pyrite thin films for solar cells application, Journal of Materials Science: Materials in Electronics 30 (2019) 19752–19759. https://doi.org/10.1007/S10854-019-02340-7.

[76] G. Han, S. Wen, H. Wang, Q. Feng, Interaction mechanism of tannic acid with pyrite surfaces and its response to flotation separation of chalcopyrite from pyrite in a low-alkaline

medium, Journal of Materials Research and Technology 9 (2020) 4421–4430. https://doi.org/10.1016/J.JMRT.2020.02.067.

[77] N. Bhardwaj, P. Sharma, L. Guo, O. Dagdag, V. Kumar, Molecular dynamic simulation, quantum chemical calculation and electrochemical behaviour of Punica granatum peel extract as eco-friendly corrosion inhibitor for stainless steel (SS-410) in acidic medium, J. Mol. Liq. 346 (2022) 118237. https://doi.org/10.1016/J.MOLLIQ.2021.118237.

[78] Q. Wang, H. Zheng, L. Liu, Q. Zhang, X. Wu, Z. Yan, Y. Sun, X. Li, Insight into the anti–corrosion behavior of Reineckia Carnea leaves extract as an eco–friendly and high–efficiency corrosion inhibitor, Ind. Crops Prod. 188 (2022) 115640. https://doi.org/10.1016/J.INDCROP.2022.115640.

[79] C. Merimi, B. Hammouti, K. Zaidi, B. Hafez, H. Elmsellem, R. Touzani, S. Kaya, Acetylsalicylic acid as an environmentally friendly corrosion inhibitor for carbon steel XC48 in chloride environment, J. Mol. Struct. 1278 (2023) 134883. https://doi.org/10.1016/J.MOLSTRUC.2022.134883.

[80] Q. Wang, L. Liu, Q. Zhang, X. Wu, H. Zheng, P. Gao, G. Zeng, Z. Yan, Y. Sun, Z. Li, X. Li, Insight into the anti–corrosion performance of Artemisia argyi leaves extract as eco–friendly corrosion inhibitor for carbon steel in HCl medium, Sustain. Chem. Pharm. 27 (2022) 100710. https://doi.org/10.1016/J.SCP.2022.100710.

[81] F.Z. Eddahhaoui, A. Najem, M. Elhawary, M. Boudalia, O.S. Campos, M. Tabyaoui, A. José Garcia, A. Bellaouchou, H.M.A. Amin, Experimental and computational aspects of green corrosion inhibition for low carbon steel in HCl environment using extract of Chamaerops humilis fruit waste, J. Alloys Compd. 977 (2024). https://doi.org/10.1016/j.jallcom.2023.173307.

[82] A.T.J. Rani, A. Thomas, M. Arshad, A. Joseph, The influence of aqueous and alcoholic extracts of Garcinia cambogia fruit rind in the management of mild steel corrosion in hydrochloric acid: Theoretical and electroanalytical studies, J. Mol. Liq. 346 (2022) 117873. https://doi.org/10.1016/J.MOLLIQ.2021.117873.